Distortion and Segregation in a Dislocation Core Region at Atomic Resolution

X. Xu,[1,2] S. P. Beckman,[1,3,†] P. Specht,[1] E. R. Weber,[1,3] D. C. Chrzan,[1,3] R. P. Erni,[4] I. Arslan,[4]
N. Browning,[2,4] A. Bleloch,[5] and C. Kisielowski[2,*]

[1]*Department of Materials Science and Engineering, University of California, Berkeley, California 94720, USA*
[2]*National Center for Electron Microscopy, Lawrence Berkeley National Laboratory, Berkeley, California 94720, USA*
[3]*Material Science Division, Lawrence Berkeley National Laboratory, Berkeley, California 94720, USA*
[4]*Department of Chemical Engineering and Materials Science, University of California, Davis, California 95616, USA*
[5]*UK SuperSTEM, Daresbury Laboratory, Daresbury, Cheshire, WA4 4AD, United Kingdom*
(Received 17 February 2005; published 28 September 2005)

The structure of an isolated, Ga terminated, 30° partial dislocation in GaAs:Be is determined by high resolution transmission electron microscopes and focal series reconstruction. The positions of atomic columns in the core region are measured to an accuracy of better than 10 pm. A quantitative comparison of the structure predicted by an *ab initio* electronic structure total energy calculation to the experiment indicates that theory and experiment agree to within 20 pm. Further analysis shows the deviations between theory and experiment appear to be systematic. Electron energy loss spectroscopy establishes that defects segregate to the core region, thus accounting for the systematic deviations.

DOI: 10.1103/PhysRevLett.95.145501 PACS numbers: 61.72.Ff, 79.20.Uv

The core of a dislocation often controls the properties of the dislocation, including mechanical and electronic behaviors. In spite of nearly 50 years of research, dislocations in semiconductors still exhibit unexplained features related to core reconstructions, kink motion, and impurity segregation [1–4]. Although a great number of studies have been aimed at understanding the core structures of dislocation in semiconductors, much is still unknown [5]. Linear elasticity theory describes the far-field displacements associated with dislocations remarkably well [6] but *cannot* describe the displacements within the dislocation core itself. Existing studies exploit dislocation arrays to measure core properties, but interactions between dislocations may distort the core structures and segregation patterns of the individual dislocations [7,8]. Only recently has electron microscopy become capable of resolving the dislocation core structure to an atomic level [9–13]. It is desirable to observe directly the structure of the dislocation core to the atomic level; however, in diamond cubic and *zincblende* semiconductors resolving dumbbell atom columns along the dislocation line requires a resolution better than the typical Scherzer point resolution of $\sim$0.18 nm of most high resolution transmission electron microscopes (HRTEM) [14]. As a result, investigations of dislocations are often indirect [15,16] or utilize other experimental techniques such as scanning tunneling microscopy [17] or imaging with forbidden reflections [18]. In this Letter, we have applied phase contrast electron microscopy, which allows for direct study of defect structures with sub-Ångstrom resolution [12,13], in combination with scanning transmission electron microscopy (STEM), which enables local spectroscopy to be performed at an atomic level [19–21], and density functional theory based calculations [22] to describe an isolated partial dislocation in GaAs.

Dislocations in *zincblende* crystals prefer to lie along the valleys of the Peierls energy in the $\langle 110 \rangle$ directions and glide on the $\{111\}$ planes. The dislocations dissociate into Shockley partials separated by an intrinsic stacking fault (ISF). The resulting partial dislocations have Burger's vectors that are either 30° or 90° inclined to the line direction. If the extra half plane of atoms associated with the partial dislocation terminates on an As atom that lies in the narrowly spaced planes, called the *glide set* planes, the dislocation is of α type. If it terminates on a Ga atom in the glide set configuration, it is called a β dislocation.

Electron transparent samples were prepared from a GaAs:Be crystal, $[\mathrm{Be}] = 2 \times 10^{21}$ cm^{-3}, grown by molecular beam epitaxy at 224 °C. The lattice parameter remained that of natural GaAs, 5.65 Å. Dislocation and $\mathrm{As_{Ga}}$ antisite defects were measured at concentrations of 10^9 cm^{-2} and 2×10^{20} cm^{-3}, respectively [23]. Specimens with $[011]$ surfaces were prepared in cross section geometry and thinned by low voltage (500 V)/low angle (6°) Ar ion milling to electron transparency.

A focal series of lattice images was recorded using a CM300 FEG/UT, a 300 kV microscope equipped with a field emission electron source (FEG) and ultratwin (UT) objective lens, that has an information limit of $\sim$0.08 nm [12,13]. A. holographic technique was applied to reconstruct the complex electron exit wave using the TRUEIMAGE software package [24,25]. The reconstruction method leaves the image unfiltered across a contrast transfer function that ranges from 2 to 12.5 nm^{-1}. Lens aberration corrections were applied since they influence the location of intensity maxima relative to column positions. Twofold and threefold astigmatism as well as coma were corrected to better than 1, 50, and 50 nm, respectively. Other lens aberrations, such as fourfold or higher astigmatism were neglected. Such residuals reduce the mismatch between

 © 2005 The American Physical Society

intensity maxima and column positions to pm values. To our knowledge no other imaging process can provide a similar precision at sub-Angstrom resolution.

Figure 1(a) shows the phase of a reconstructed electron exit wave of a partial dislocation with its associated ISF. By Burger's circuit analysis the dislocation is identified as a 30° partial. A contrast comparison of dumbbell column pairs as a function of the sample thickness allows for identification of the atom species since the heavier As atoms scatter the electron beam stronger. Thereby, the dislocation core was found to be a Ga terminated 30° β partial dislocation, which is confirmed by the image simulation of Fig. 2.

Figure 1(b) shows an incoherent high angle annular dark field (HAADF) STEM image of an ISF (at a different position) in this same material. The HAADF image was obtained at the superSTEM laboratory in the UK on a VG HB501 dedicated STEM fitted with a second generation spherical aberration corrector, a spectroscopy-coupling module (both manufactured by Nion Co.), and a Gatan Enfina electron energy loss spectrometer. The spectroscopy-coupling module is necessary to compress the angular range of the bright field disk (which is large due to the convergence angle required for the 0.1 nm resolution) so that the 2 mm entrance aperture to the spectrometer can collect a reasonable fraction of the electrons that pass through the sample while maintaining 0.4 eV spectral resolution. Particular care was taken with the environment of the instrument resulting in a spatial resolution of 0.1 nm with about 60 pA probe current and a drift stability of 0.05 nm in 100 s. The convergence semiangle of the electron probe was 24 mrad for both imaging and spectroscopy. The collection semiangle for the EELS spectra was 15 mrad and for the HAADF imaging was 70 to 200 mrad. Using this imaging method in an aberration corrected microscope [19] allows a 1 Å electron probe to be located at regions of interest to perform electron energy loss spectroscopy (EELS) [20]. At each probe position [indicated by circles in Fig. 1(b)] local spectra of the As and Ga L2/3 edges, Be and C (used for calibration) K edges were recorded. Their intensity ratios (As/Ga, Be/C) are shown in the inset of Fig. 1(b). The spectra reveal that there is Ga and Be enrichment at the stacking fault.

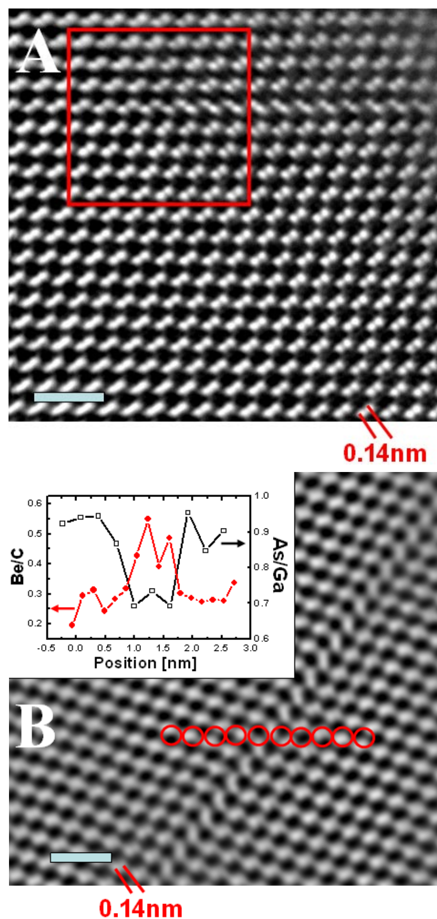

FIG. 1 (color online). Atomic resolution images of defects in GaAs. In the images, the scale bar represents 0.5 nm and a As-Ga dumbbell distance is indicated. (a) Reconstructed phase image of a 30°-Beta-partial dislocation with adjacent ISF in GaAs generated from a focal series of lattice images. The resolution limit is 0.08 nm. (b) HAADF STEM image of an ISF in GaAs recorded with a 0.1 nm probe. The circles indicate the probe position during EELS measurements. The inset shows the relative concentrations of As/Ga (square) and Be/C (circle) from EELS measurement.

The atomic structure of the dislocation was predicted by the *ab initio* total energy method as implemented in VASP [26–28]. The details of the computational method can be found elsewhere [22]. The *ab inito* calculation was designed to simulate the properties of an isolated partial dislocation in bulk GaAs. Using the MACTEMPAS software package, a focal series of lattice images was simulated from the predicted structure and reconstructed with the TRUEIMAGE software package. This process was optimized with geometrical aspects to match the experiment and establish the column positions to within 10 pm. In the

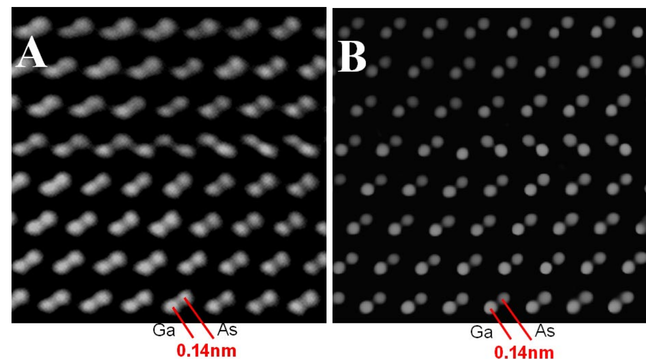

FIG. 2 (color online). Magnified phase image of core and stacking fault from (a) experimental HREM image in Fig. 1(a) and (b) simulated HREM image generated from a calculated atomic structure. The location of As and Ga columns are known from simulations. Simulated intensities compare well with the experimental data revealing the presence of a Ga terminated core.

images, the positions of individual columns were identified by simultaneously fitting two Gaussian functions to the intensities of each dumbbell (As-Ga) column pair [29] in the two-dimensional image plane. For comparison with experiment, the atomic structure was scaled to correct for the well-known discrepancy between predicted and measured bulk lattice parameters. Figures 2(a) and 2(b) show a comparison of the reconstructed phase image of Fig. 1(a) with an equivalent simulated reconstructed electron exit wave of the predicted structure. Since the TEM sample was of finite thickness, a correction for relaxation caused by the Eshelby twist [30] of the screw component was applied to the calculated atomic structure, yielding additional displacements of the order of 1–10 pm.

In addition to the surface correction, sample tilt with respect to the electron beam was also observed during comparison of the simulation to experiment. The magnitude of the tilt was 0.2 degrees. This is related to the inability to focus the 300 kV electron beam directly on the dislocation core without causing radiation damage. Coupling of the Eshelby twist to the sample tilt introduces the loss of contrast as shown in the second quadrant of Fig. 2. This artifact could not have been identified accurately without comparison of theoretical and experimental methods.

The mismatch between the calculated and measured atom positions is plotted in Fig. 3(a) as a vector field. Over most of the image it is ≤ 8 pm, while in the immediate core region and along the stacking fault it can be as large as 18 pm. One can alter column positions considering bond length variations due to impurity segregation to reduce the amplitude of the mismatch to below 10 pm everywhere [see Fig. 3(b)]. This implies that site-specific point defect segregation takes place and can be revealed by displacement measurements with pm precision. A physical background and detailed values are given next.

Repetitive measurements of the 1.41 Å dumbbell distance in the bulk of the material reveal a precision of $2\sigma = 4.8$ pm for the measurement of individual column positions that is small enough to verify an elongation of that distance to a mean of 1.58 Å if measured along the ISF as shown in Fig. 4(a). An increased standard variation of the ISF data, $2\sigma = 20$ pm, indicates the presence of an underlying physical process with local variation. *Ab initio* calculation of the stacking fault structure predicts a dumbbell length of 1.41 Å, which is identical to the bulk value. A similar situation to that observed in the HREM is recorded in the HAADF image of Fig. 1(b) and analyzed in Fig. 4(b). Again, the dumbbell distance expansion reaches a mean of 1.6 Å along the ISF. The lower precision of this measurement relates to less resolution and higher scan noise in the HAADF image, which increases errors in the fitting procedure that is used for position determination. Since this image shows the same effect as the phase image, the bond length elongation at the ISF is reproduced and linked to the possible segregation of Ga and Be.

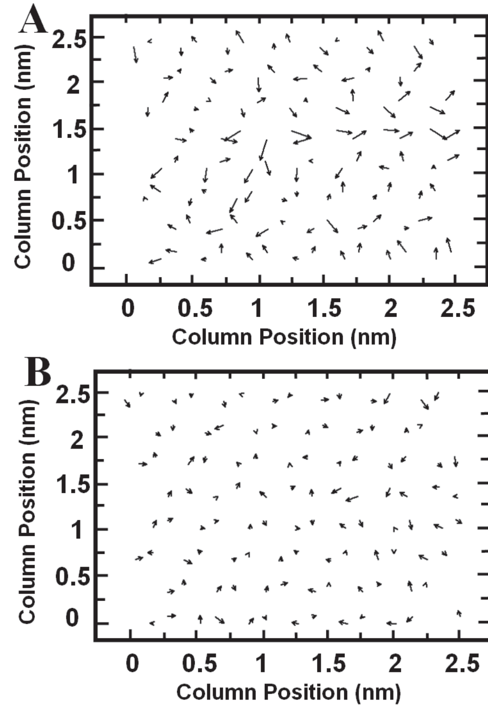

FIG. 3. Vector plots showing magnitude and direction of deviations between experimental and simulated atomic column positions. (a) The mismatch between columns is less than 8 pm outside core region and reaches 18 pm at the core. (b) A mismatch of less than 10 pm everywhere can be obtained by allowing for projected bond length variations on a 10 pm level that can be generated by site-specific defect segregation.

The positive element identification suggests that Be may segregate to As sites at the stacking fault, thereby increasing the Be concentration while simultaneously depleting the As. However, even a 100% occupation of the As sites with Be atoms results in a projected As-Ga dumbbell distance of only 1.42 Å, which is smaller than the observed expansion, suggesting that this is an unlikely cause. Another possible explanation is the segregation of Be to Ga sites and of Ga to As sites. The dumbbell length computed for this pair structure is 1.53 Å, which is only 3% smaller than the measured expansion and within accuracy limits of the computational method. The effect of placing other impurities and antisite defects at the fault was also investigated, but none offered closer agreement with the experiment than the modeled pair substitution Be_{Ga}-Ga_{As}. Since our STEM measurements support Ga and Be enrichment at the ISF, we tentatively propose that Ga_{As}-Be_{Ga} pair formation can be a possible reason for the elongation of the projected bond length at the ISF. More complicated models cannot be excluded.

In conclusion, we have shown here the direct image of the core of an isolated partial dislocation in bulk GaAs:Be. A high signal to noise ratio image enables a quantitative comparison between experiment and simulation. It has been demonstrated how the coupling of theory and experiment can be used to identify the effects of Eshelby twist

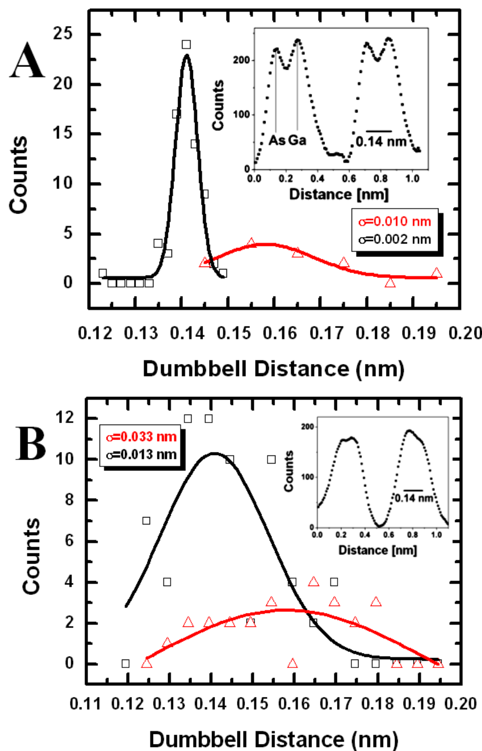

FIG. 4 (color online). Histogram showing the number of dumbbell bonds of given length at the ISF and in the bulk for (a) HREM image shown in Fig. 1(a). (b) STEM image shown in Fig. 1(b). (Squares: measured off the ISF; triangles: measured on the ISF). Insets show line traces across the dumbbell structure of Fig. 1 proving that in both cases single column resolution could be achieved.

and off-axis tilting. The positions of atom columns can be determined experimentally to a precision $2\sigma = 4.8$ pm. Column positions predicted by an *ab initio* electronic structure total energy method and extracted from the phase of the complex electron exit wave agree to better than 20 pm within the dislocation core and along the intrinsic stacking fault if a stoichiometric partial dislocation is modeled. The agreement is better then 8 pm everywhere else in the image. Systematic deviations between experiment and calculation are attributed to site-specific defect segregation that is observed directly using EELS. Thereby, in this Letter, we show that a suitable combination of imaging, local spectroscopy, and modeling allows for a full characterization of an individual dislocation core and stacking fault including segregation effects.

We thank R. Kilaas for helpful discussions. D. C. C. acknowledges the support of the Miller Institute for Basic Research. This research used resources of the Laboratory Technology Research Division (SC-32), within the Office of Science, US Department of Energy under a CRADA (Cooperative Research and Development Agreement) between Lawrence Berkeley National Laboratory (LBNL) and Lumileds Lighting, San Jose/CA. This research is also supported by the National Energy Research Scientific Computing Center and the Directorate, Office of Science, Office of Basic Energy Sciences, of the US Department of Energy and the Air Force Office of Scientific Research.

*Corresponding author.
Present address: National Center for Electron Microscopy, Lawrence Berkeley National Laboratory, BLDG 72-150, 1 Cyclotron Road, Berkeley, CA, 94706, USA.
Fax: +1-510-486-4846
Phone: +1-510-486-4716 (office)
Email address: CFKisielowski@lbl.gov
†Present address: The Institute for Computational Engineering and Sciences, University of Texas, Austin, Texas 78712, USA.

[1] H. Alexander and H. Teichler, in *Dislocations in Handbook of Semiconductor Technology*, edited by K. A. Jackson and W. Schröter (Wiley-VCH, Berlin, 2000), Vol. 293–376.
[2] H. J. Queisser and E. E. Haller, Science **281**, 945 (1998).
[3] E. R. Weber, Physica (Amsterdam) **340-342B**, 1 (2003).
[4] F. Louchet and J. Thibault-Desseaux, Rev. Phys. Appl. **22**, 207 (1987).
[5] R. Jones, Mater. Sci. Eng. B **71**, 24 (2000).
[6] M. J. Hÿtch, J. L. Putaux, and J. M. Pénisson, Nature (London) **423**, 270 (2003).
[7] S. H. Lim *et al.*, Phys. Rev. Lett. **81**, 5350 (1998).
[8] X. Blasé *et al.*, Phys. Rev. Lett. **84**, 5780 (2000).
[9] S. Lopatin *et al.*, Appl. Phys. Lett. **81**, 2728 (2002).
[10] A. J. McGibbon, S. J. Pennycook, and J. E. Angelo, Science **269**, 519 (1995).
[11] K. Tillmann, A. Thust, and K. Urban, Microsc. Microanal. **10**, 185 (2004).
[12] C. Kisielowski *et al.*, Ultramicroscopy **89**, 243 (2001).
[13] M. A. O'Keefe *et al.*, Ultramicroscopy **89**, 215 (2001).
[14] M. A. O'Keefe, Ultramicroscopy **47**, 282 (1992).
[15] C. Kisielowski-Kemmerich, Phys. Status Solidi B **161**, 11 (1990).
[16] C. Kisielowski and E. R. Weber, Phys. Rev. B **44**, 1600 (1991).
[17] G. Cox *et al.*, Phys. Rev. Lett. **64**, 2402 (1990).
[18] H. Alexander *et al.*, Philos. Mag. A **53**, 627 (1986).
[19] P. E. Batson, N. Delby, and O. L. Krivanek, Nature (London) **366**, 727 (1993).
[20] N. D. Browning, M. F. Chrisholm, and S. J. Pennycook, Nature (London) **366**, 143 (1993).
[21] P. E. Batson, Phys. Rev. B **61**, 16633 (2000).
[22] S. P. Beckman *et al.*, J. Phys. Condens. Matter **14**, 12673 (2002).
[23] P. Specht *et al.*, J. Vac. Sci. Technol. B **17**, 1200 (1999).
[24] W. M. J. Coene *et al.*, Ultramicroscopy **64**, 109 (1996).
[25] A. Thust *et al.*, Ultramicroscopy **64**, 211 (1996).
[26] G. Kress and J. Furthermuller, Phys. Rev. B **54**, 11169 (1996).
[27] G. Kress and J. Furthermuller, Comput. Mater. Sci. **6**, 15 (1996).
[28] G. Kress and J. Hafner, Phys. Rev. B **49**, 14251 (1994).
[29] C. Kisielowski and O. Schmidt, Microscopy and Microanalyses Suppl. 2 **4**, 614 (1998).
[30] J. D. Eshelby and A. N. Stroh, Philos. Mag. **42**, 1401 (1951).